Optical Engineering

OpticalEngineering.SPIEDigitalLibrary.org

Dimensional characterization of large opaque samples and microdeformations by low coherence interferometry

Nélida A. Russo
Eneas N. Morel
Jorge R. Torga
Ricardo Duchowicz

SPIE.

Nélida A. Russo, Eneas N. Morel, Jorge R. Torga, Ricardo Duchowicz, "Dimensional characterization of large opaque samples and microdeformations by low coherence interferometry," *Opt. Eng.* **59**(1), 014112 (2020), doi: 10.1117/1.OE.59.1.014112

Dimensional characterization of large opaque samples and microdeformations by low coherence interferometry

Nélida A. Russo,[a,*] Eneas N. Morel,[b] Jorge R. Torga,[b] and Ricardo Duchowicz[a]

[a]Centro de Investigaciones Ópticas (CONICET-CIC-UNLP), Gonnet, La Plata, Buenos Aires, Argentina

[b]UTN Facultad Regional Delta, Laboratorio de Optoelectrónica y Metrología Aplicada, Campana, Buenos Aires, Argentina

Abstract. We report on the application of an interferometric system based on the low-coherence interferometry technique to the dimensional characterization of large opaque mechanical parts as well as microdeformations experienced by them. The implemented scheme is capable of simultaneously measuring very small deformations and relatively large dimensions or thicknesses (several centimeters) of the sample. By applying the chirp Fourier transform algorithm, it was possible to measure changes in thickness with an uncertainty of 0.35 μm when a 7-cm-thick sample was measured. The measurement scheme was implemented in optical fiber, which makes it highly adaptable to industrial conditions. It employs a tunable light source and a Sagnac–Michelson configuration of the interferometric system that allows the thickness of the opaque sample and the topography of both faces to be obtained simultaneously. The developed system can be used to perform profilometry of opaque samples and to analyze the dimensional behavior of mechanical pieces in production lines or under mechanical efforts capable of introducing some deformations on them. This feature enables the system to perform quality control in manufacturing processes. [DOI: 10.1117/1.OE.59.1.014112]

Keywords: low-coherence interferometry; optical metrology; nondestructive testing.

Paper 191574 received Nov. 6, 2019; accepted for publication Jan. 8, 2020; published online Jan. 25, 2020.

1 Introduction

Low-coherence interferometry (LCI), also known as white light interferometry, is a high-resolution technique that provides accurate information on the axial position of an object in the direction of light propagation, and it is particularly useful for many industrial applications since it allows measurements to be carried out accurately, quickly, and noninvasively.[1] Moreover, LCI has found widespread use in optical low-coherence reflectometry, which forms the basics of optical coherence tomography (OCT), a method allowing nondestructive investigation of internal structure of a broad range of biological and technical samples.[2] In recent years, LCI has been used as a tool in the development of nondestructive testing equipment, and increasingly research groups are dedicated to exploring new applications. Thus, for example, it was used to build up a high sensitivity instrument for intraocular distance measurement of the human eye *in vivo*,[3] in the development of a system and a method that is able to identify different tissue types,[4] to measure microscopic brain motions *in vivo*,[5] for measuring the group refractive indices of dispersive samples of unknown thickness,[6] to perform the wavelength calibration of dispersive spectrometers,[7] among others.

In the first versions of the time-domain OCT, developed during the 1990s, the interference signal was generated by the displacement of the mirror in the interferometer reference arm. When this method was employed to measure distances >1 cm, it was necessary to use a precise

*Address all correspondence to Nélida A. Russo, E-mail: nelidar@ciop.unlp.edu.ar

0091-3286/2020/$28.00

mechanical system, which turned measurements into a slow and relatively expensive process.[8] Subsequently, techniques in the frequency-domain LCI (FD-LCI) and frequency-domain OCT were developed that allowed the design of more robust, compact, and faster systems.[9–12] In this technique, it is not necessary to move the mirror, and detection is performed using a diffractive spectrometer. However, the use of this detector limits the maximum value of measurable optical path difference (OPD). This value depends on the number of lines per mm of the diffraction grating and the number and size of the spectrometer sensor pixels. Normally, the maximum OPD value is <1 cm. In addition, in spectrometer-based OCT systems, the signal sensitivity tends to be weaker in regions of deeper images, which is called depth-dependent sensitivity fall-off. It depends largely on the characteristics of the spectrometer, such as pixel size, angular dispersion of wavelengths, and focus point. The reduction of the sensitivity drop is one of the main concerns in the design of a spectrometer for an FD-LCI system.[13]

Since many industrial applications involve the measurement of distances >1 cm, it is relevant to be able to increase the maximum measurable value of OPD. The solution to these limitations is the use of tunable lasers that provide a coherence length much greater than the light sources typically used in LCI, allowing to extend the measurement range to more than 1 m.[14] However, this does not resolve the limitation that arises from the use of Michelson interferometers when it is desired to measure the thickness of an opaque object. Since these schemes can only measure one sample's face at a time, it will also be necessary to use a reference surface. One possible solution is the simultaneous use of a Sagnac ring interferometer.[15] This type of interferometer allows the simultaneous illumination of both sides of the sample allowing to determine the surface characteristics and the absolute dimension of the object.

Finally, it should be mentioned that, when the system is implemented using optical fiber, low-coherence interferometers can perform remote measurements whose results are independent of external disturbances. In addition, it is rugged enough to be used in industrial or harsh environments, and the optical probe can be miniaturized to access narrow or hard-to-reach places. On the other hand, in industrial applications, real-time measurements and simplicity in the experimental setup are much appreciated, even at the expense of worsening the resolution to achieve this goal.

In this paper, we show the application of an interferometric system based on the LCI technique to perform thickness measurements in large opaque samples or where the refractive index is unknown. It should be noted that when working with a semitransparent multilayer sample, more reflection and transmission interfaces appear, which generate new interference signals located at different distances.[16] In this case, a preliminary analysis is performed to determine the amount of interference signals that should appear.

The measurement scheme is based on a Sagnac–Michelson configuration implemented in optical fiber. It employs an erbium-doped fiber laser tunable in the 1550-nm spectral region as the light source, and it includes a self-calibration stage that allows monitoring of the spectral position of the laser emission in each scan.[17] The developed system has a wide measuring range (several centimeters) and good axial resolution, which allows performance of dimensional inspection applications in different industrial areas. The results obtained by measuring different opaque samples up to about 7-cm thick are shown, as well as the microdeformations experienced by a sample subjected to pressures up to 6 atm above normal atmospheric pressure. It is important to note that the implemented scheme is capable of simultaneously measuring small deformations compatible with the system resolution at the same time as relatively large dimensions or thicknesses. The simplicity of the proposed configuration privileges aspects such as robustness, reliability, and repeatability, which makes it appropriate for use in the dimensional characterization of large mechanical parts as those used in different industrial fields.

2 Discussion

2.1 *Experimental Setup*

The principal objective of interferometry is the measurement of the OPD between interfering beams and determination of the values of the physical quantities which give rise to measured

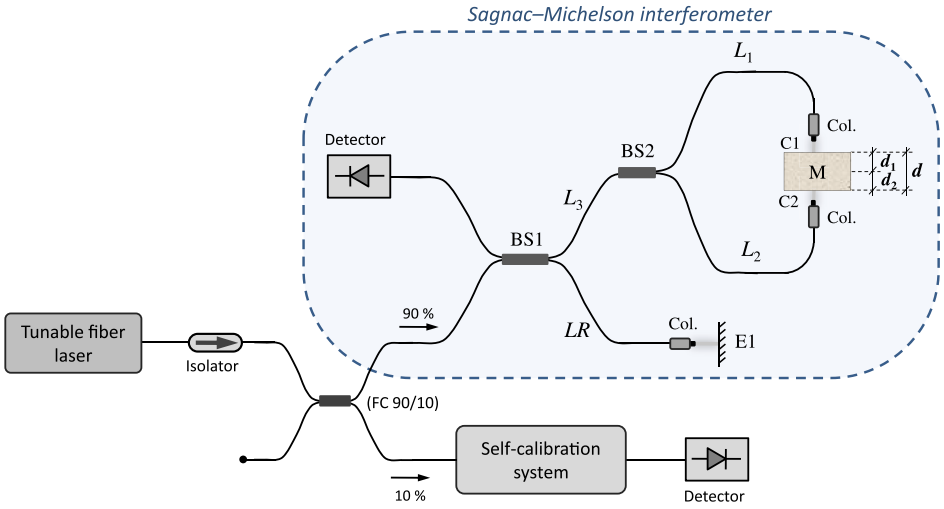

Fig. 1 Experimental setup proposed to measure opaque samples with the Sagnac–Michelson interferometer implemented in optical fiber.

OPD. The optical configuration of a typical LCI system based on fiber optics uses a 2×2 fiber coupler to split the light of a low-coherence source into the sample and the reference arms of a Michelson interferometer. Light reflected in both arms is coupled back and redirected toward the detection stage where the interference pattern is recorded. Due to the finite coherence length of the light source, the interference between beams reflected in the sample and in the reference mirror is only observed when the OPD among them is less than the coherence length of the light source. This also causes the interference pattern to be modulated by an envelope function dependent on the coherence function of the source, which limits the measurement depth.

For the measurement of opaque samples, it is necessary to modify such arrangement and use a configuration based on a combination of the Michelson and the Sagnac interferometers. This configuration allows the determination of thicknesses of opaque samples or whose refractive index is unknown, as well as surface characterization of nontransparent objects (profilometry of mechanical parts). Figure 1 schematically shows the proposed measuring system, with the Sagnac–Michelson interferometer implemented in optical fiber. E1 is the mirror of the reference arm, while BS1 and BS2 are the beam splitters implemented with fused fiber optic couplers with a coupling ratio 50:50. The beams that illuminate the mirror in the reference arm and each side of the sample are collimated by means of single mode gradient-index (GRIN) fiber optic collimators (Col.). The ring that is formed at the output of BS2 with the beams that illuminate the sample defines the Sagnac configuration.

The path performed by the light beam can be described as follows. After the first splitter (BS1), one beam travels toward the reference mirror (E1) and the other toward the second splitter (BS2), where it is separated again into two beams, each of which illuminates opposite faces of the sample. Upon reaching the sample (M), the beams are reflected and perform the reverse way. The reflections on the three surfaces (the mirror E1 and the two faces of the sample C1 and C2) are superimposed on the detector and produce the interference signal containing the information of interest (the thickness of the sample in the direction of illumination).

The OPDs between the distances traveled by the different light beams generate the modulations in the interference signal, which are analyzed in the Fourier space. From this analysis, the OPDs can be determined in each case by obtaining the position of the maximum of the "interference peak" in the Fourier transform.

We will call: P_r the position (in the OPD axis) of the peak corresponding to the term (or component) of the interference signal generated by the reflection at E1 (reference beam) and the beam traveling through the Sagnac interferometer when there is no sample (and with the corresponding collimators aligned); P_1 the peak that is produced by the interference between the reference beam and the reflection on the face C1 of the sample; P_2 the peak that arises from the interference between the reference and the reflection on the other side of the sample

(C2). The distances L_i represent the paths traveled by the light in the different sectors of the interferometer (see Fig. 1), that is, L_1 is the optical path between BS2 and the face C1 of the sample, L_2 is the optical path between BS2 and the face C2 of the sample, L_3 is the optical path between BS1 and BS2, LR is the length of the reference arm (between BS1 and E1), and d is the thickness of the sample. In addition, d_1 and d_2 are the segments of the thickness of the sample (d) on each side of the axis of symmetry of the Sagnac interferometer. Therefore,

$$d = d_1 + d_2, \tag{1}$$

$$P_r = 2\mathrm{LR} - (2L_3 + L_1 + L_2 + d), \tag{2}$$

$$P_1 = 2\mathrm{LR} - 2(L_3 + L_1), \tag{3}$$

$$P_2 = 2\mathrm{LR} - 2(L_3 + L_2). \tag{4}$$

By operating with the above equations, it is possible to determine the thickness of the sample under study from

$$(P_1 + P_2) - 2P_r = 2d. \tag{5}$$

As P_1 and P_2 are the OPDs between the sample faces and a reference plane, a lateral displacement of the sample let us to obtain the surface topography of each face. It is interesting to note that it was not necessary to make considerations regarding the lengths that the interferometer branches should have or the position of the sample, so that Eq. (5) is general and can be used in any condition. For example, a variation in the position of the sample in the direction of light propagation does not modify the d value because when P_1 is modified, P_2 is modified in the same absolute value but with the opposite sign, so the d value remains unchanged. This is an important feature of the implemented configuration, which makes it insensitive to vibrations in the direction of light propagation. The signs of the interference peaks depend on how the faces of the object are located relative to the axis of symmetry of the ring interferometer, as well as their position with respect to the reference plane. A complete analysis of these considerations can be found in Ref. 15.

The implemented measuring system employs a continuous wave emission erbium-doped fiber laser, tunable in a spectral range from about 1520 to 1570 nm using a variable-spaced Fabry–Perot filter having a free spectral range of 60 nm and a bandwidth of 60 pm. Sweeping is achieved by applying a periodical signal such as a triangular voltage waveform to the filter cavity piezoelectric (PZT) actuator. An appropriate selection of the doped fiber length allows one to obtain a good flatness of the spectral emission. When the laser operates at any fixed wavelength within the tuning range, the emission spectrum has a typical width of 20 pm at 3 dB.[18]

In OCT, the width at half-height of the Fourier transform of the light source spectrum is called resolution. This value indicates the minimum difference necessary to be able to identify two thicknesses simultaneously when a tomography is performed. In addition, it indicates the smallest thickness that can be measured. This is because the interference signal has a continuous component (DC) that in the transformed space generates a peak located at the origin of coordinates. For this reason, the dynamic range is usually defined by taking this value as the lower limit.

In the case of LCI, this value indicates precisely this last idea. In our system, that minimum measurable value is 21 mm and is derived from

$$R_{\mathrm{lim}} = \frac{2\ \ln(2)}{\pi}\frac{\lambda_0^2}{\Delta\lambda}, \tag{6}$$

where λ_0 is the central wavelength of the laser source and $\Delta\lambda$ is the spectral width of the tuning range. When it is necessary to perform profilometry by applying LCI technique, the ability to distinguish a shift of the interference peak in some direction can be increased using different techniques widely disseminated in the literature, such as zero padding or chirp Fourier transform. This increases the amount of points used in the Fourier transform, allowing better determination

of the shape of the interference peaks and their positions.[15] By applying these algorithms, it was possible to measure changes in thickness in the order of the micrometer with an error (or standard deviation) of 0.35 μm. The uncertainty or error value in each measurement performed with our system arose from considering the standard deviation of a series of measurements made repeatedly on the same sample. The process was carried out on samples with different thicknesses and in all cases the uncertainty values obtained were coincident.

The tunable laser employed in this work has sufficient coherence length to allow the formation of great depth images. The measurement depth, i.e., the theoretical maximum distance, that the system can measure ($\Delta z_{\max}$) is determined by

$$\Delta z_{\max} = \frac{\lambda_0^2}{4 n_g \delta_\lambda}, \tag{7}$$

where n_g is the group refractive index of the medium, in which light is propagated and δ_λ is the spectral width of the laser emission when it is sweeping in wavelength (somewhat larger than that corresponding one when it is operating at any fixed wavelength within the tuning range). For the tunable laser source used in our measuring system, it can be considered $\delta_\lambda = 30$ pm so, theoretically $\Delta z_{\max} = 20$ cm. However, due to the divergence of the collimators used in the setup and the coherence length of the light source, a drop in the visibility of the interference signals occurs as the OPD increases. This leads to a decrease in the amplitude of the corresponding interference peaks which produces the degradation of the signal-to-noise ratio and limits the maximum measurable distance to a value ($\sim$17 cm) slightly below the theoretical maximum previously mentioned.

In the proposed experimental system, the lateral resolution is determined by the radius of the spot at the point where the beam is reflected on the surface of the sample. This is defined by the characteristics of the collimation optics employed (lenses C1 and C2, Fig. 1). In this work, GRIN fiber optic collimators, model 50-1550A-APC by Thorlabs, were used. This optic is particularly suitable for use with small diameter beams and has low chromatic aberration in a range of wavelengths between 1250 and 1650 nm.

On the other hand, to avoid an inherent problem of sweeping sources which is related with certain uncertainties that arise from the nonlinear movement of the PZT used to tune the laser, we used a passive self-calibration stage based on fiber Bragg gratings (FBG) of known spectral positions.[16,17] This allowed counteracting the possible variation in the scanning speed of the laser caused by the tuner module, in addition to linking the emission wavelength of the laser and the temporal position in each sweep, transforming the temporal axis into an axis in wavenumber (k). The central wavelengths of the FBGs employed in our work were 1527.84, 1535.73, 1541.82, 1547.65, 1553.62, and 1558.43 nm, and their spectral widths were in the order of 0.1 nm. Since the spectral locations of the FBGs were known, from the measurement of their temporal positions, it was possible to calibrate the measurement system, resizing for each sweep of the source the time axis provided by the oscilloscope used to acquire the signal. The sequence of values k_{FBGi} (wavenumber corresponding to the i'th Bragg filter) and the associated times (t_{FBGi}) allowed to obtain a curve that could be interpolated to find the function $k(t)$ that relates the sampling times to a uniformly sampled k-space. From there, the sampling frequency to be used in the calculation of the Fourier transform of the registered signals was obtained.

The temporal distribution of the optical intensity corresponding to the interference signal was obtained using an InGaAs photodetector with 2-GHz bandwidth in conjunction with a digital oscilloscope, although it can be replaced by any 200-MHz bandwidth digitizer or digital to analogue converter system with two acquisition channels. Then, the Fourier transform was applied to the detected signals and the position of the interference peaks allowed obtaining the thickness of the opaque sample by applying the procedure explained before. Figure 2 shows a typical record of (a) the interferometric signal that contains the dimensional information of the sample and (b) the calibration signal with FBG attenuation peaks used to relate the emission wavelength of the source and the temporal position in each sweep.

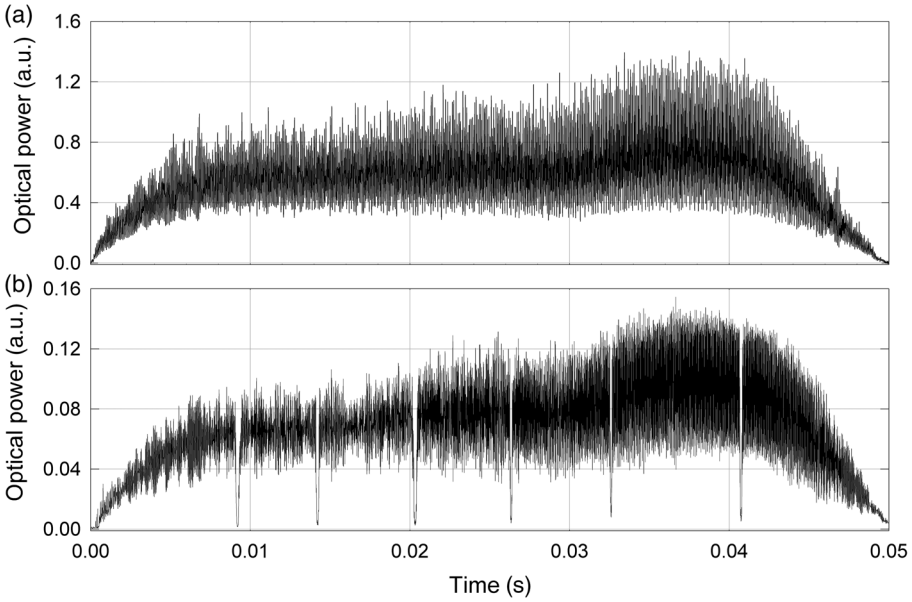

Fig. 2 Typical records obtained with an oscilloscope when measuring the thickness of an opaque sample. (a) Interferometric signal and (b) calibration signal.

2.2 *Deformation Measurement*

In certain applications, it is usually necessary to measure microdeformations produced in large objects. As an example, we will consider those experienced by diaphragms under the action of intermediate working pressures. To apply the developed system in the measurement of this type of deformations, a hollow aluminum cylinder was constructed with its ends tightly closed by means of brass (copper and zinc alloy) caps. The aluminum walls are thick enough not to deform by applying inside the cylinder the pressure levels used in this work, while the flat faces of the end caps are thin enough to undergo deflection. These caps have different thicknesses so it was expected that they would have a different dynamic behavior. Subsequently, pressurized air was injected by means of a standard pneumatic compressor inside the hermetically sealed cylinder. The pressure was varied and the deformation experienced in each case by the flat walls of the caps was measured using the interferometric system shown in Fig. 1. To model the behavior of each of these surfaces when injecting pressurized air into the cylinder, it can be considered the deformation experienced by a circular plate fixed in its contour under the action of a uniformly distributed vertical load,[19,20] as shown in Fig. 3.

The transverse deflection of the plate as a function of the distance to the center $[w(r)]$ depends on its material properties, geometric properties, and boundary conditions, as well as the magnitude of the applied load, and can be expressed as

$$w(r) = \frac{Pa^4}{64D}\left[1 - \left(\frac{r}{a}\right)^2\right]^2, \tag{8}$$

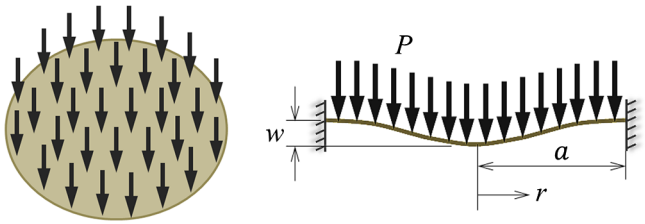

Fig. 3 Static deformation experienced by a circular plate with fixed outer edges under the action of a uniformly distributed vertical load.

where $D = Eh^3/12(1 - v^2)$ is the flexural rigidity of the plate, E and v are the Young's modulus and the Poisson's coefficient of the material, respectively, a is the radius of the circular plate, h is its thickness, r is the position of the deformation, and P is the applied transverse load per unit area. The maximum deformation occurs in the center of the plate ($r = 0$). In the modeling used to calculate the deformation experienced by the plate, the following assumptions are considered: (1) the plate is flat, of uniform thickness, and of homogeneous isotropic material; (2) the thickness is not more than about onequarter of the least transverse dimension, and the maximum deflection is not more than about one-half the thickness; (3) all loads and reactions are normal to the plane of the plate; and (4) the plate is nowhere stressed beyond the elastic limit.

3 Experimental Results

In our experiments, the interferometric system was used to measure the thickness of different opaque objects and the deformation experienced by a hollow piece when applying pressure inside it. The results of the measurement of eight aluminum cylinders shown in Fig. 4, of different thicknesses between 5 and 50 mm are shown below. For each of the samples, the following was recorded: (1) the interferometric signal obtained with the reference and the Sagnac ring without the object; (2) the interferometric signal with the object placed inside the Sagnac ring and the reference. This allows to obtain the OPDs corresponding to the peaks P_r, P_1, and P_2 of Eq. (5) from which it is possible to determine the thickness d of the object as previously explained. In Fig. 5, the Fourier transforms corresponding to both situations for one of the samples are observed, resulting in a thickness $d = 30.03975$ mm. The AP12 peak always appears in this type of measurements and is the OPD between each of the faces of the sample, that is,

Fig. 4 Opaque objects used to measure different thicknesses with the implemented system.

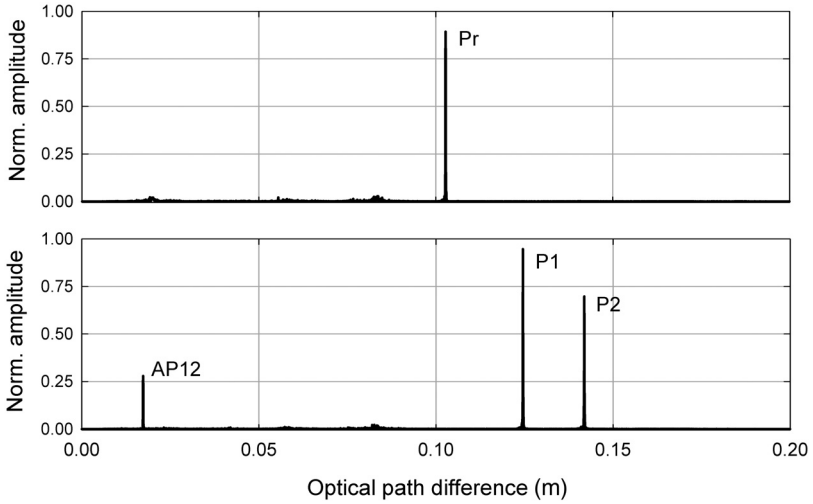

Fig. 5 Fourier transforms of the interference signals obtained when measuring an opaque sample of 30.03975 mm in thickness.

Table 1 Thickness of eight opaque samples measured using the developed LCI system. The uncertainty of each measurement is also indicated.

Sample	Thickness measured using LCI system (mm) $\Delta_{LCI} = \pm 0.00035$ mm
M-1	5.00434
M-2	9.95411
M-3	14.98741
M-4	20.91241
M-5	25.08297
M-6	30.03975
M-7	40.03981
M-8	50.39112

it corresponds to the interference signal between the reflections on both sides of the object, although it is not taken into account to determine its thickness. Table 1 summarizes the results obtained in determining the thickness of the mentioned samples.

In addition, Fig. 6 shows the high correspondence between the measurements made with the implemented optical system and the thickness values of the same samples obtained mechanically using a "Universal Measuring Machine" (SIP brand, model MU214B). The uncertainty of the mechanical measures was 1 μm.

As mentioned before, in order to measure the microdeformations experienced by a diaphragm when it is subjected to a certain pressure, we built a hollow aluminum cylinder (60 mm in length and 25 mm in diameter) hermetically closed at both ends with brass threaded and sealed caps, as can be seen in Fig. 7. The cylinder walls have a uniform thickness of ~8 mm, while the thicknesses of the caps were $h1 = 0.8824$ mm and $h2 = 0.6044$ mm. The applied pressure was varied between 1 and 6 atm above normal atmospheric pressure. In each case, both the total length of the device and the maximum deformation experienced by its end flat faces were simultaneously measured. The results obtained are shown in Fig. 8.

In addition, the experimental results obtained were compared with the maximum deformations calculated by applying the model and expressions mentioned in Sec. 2.2. Brass parameters ($E = 100$ GPa and $\nu = 0.33$) were used for this purpose, as well as the radius of both circular

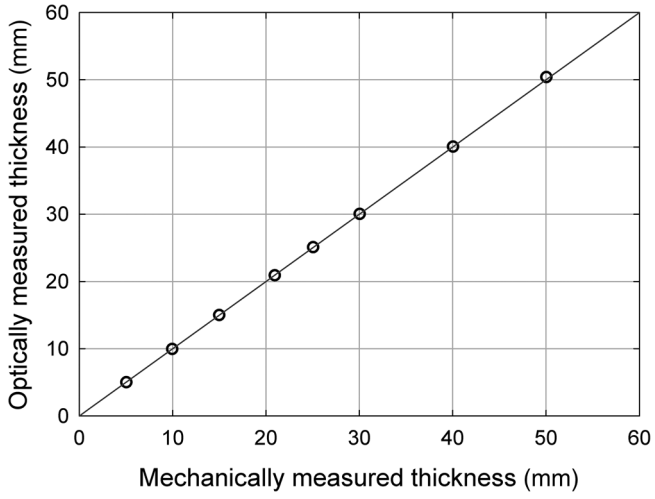

Fig. 6 Comparison between thicknesses of different samples measured optically and mechanically.

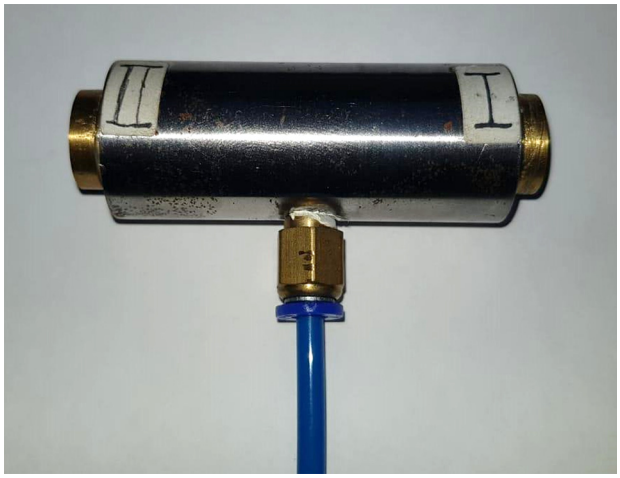

Fig. 7 Hollow object employed to measure the microdeformations experienced by its end faces when applying pneumatic pressure inside it.

plates $a = 4.5$ mm and the values indicated above for the thicknesses $h1$ and $h2$. The theoretical deformations arising from these calculations are also shown in Fig. 8(b), showing a perfect correspondence with the experimental results.

Finally, Fig. 9 shows an example of the Fourier transforms used to measure the microdeformations as well as the total length of the object by employing the implemented system. Figure 9(a) shows the interferometric signal obtained with the reference beam and the Sagnac ring without the object, whereas Fig. 9(b) displays the interferometric signal registered with the object placed inside the Sagnac ring and the reference beam, while a pressure of 6 atm

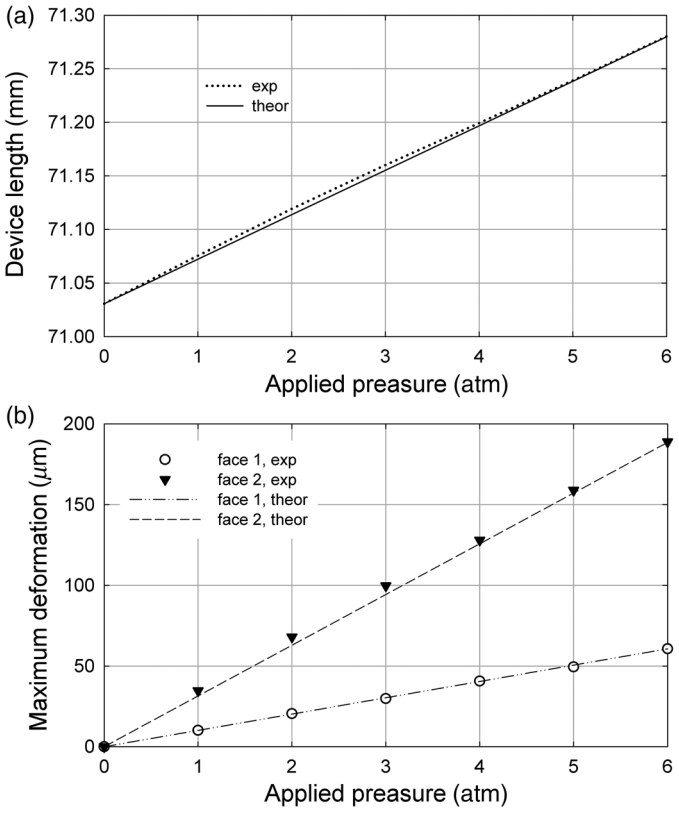

Fig. 8 (a) Total length of the device as the pressure applied inside it increases and (b) maximum deformations in the center of the flat face of each cap.

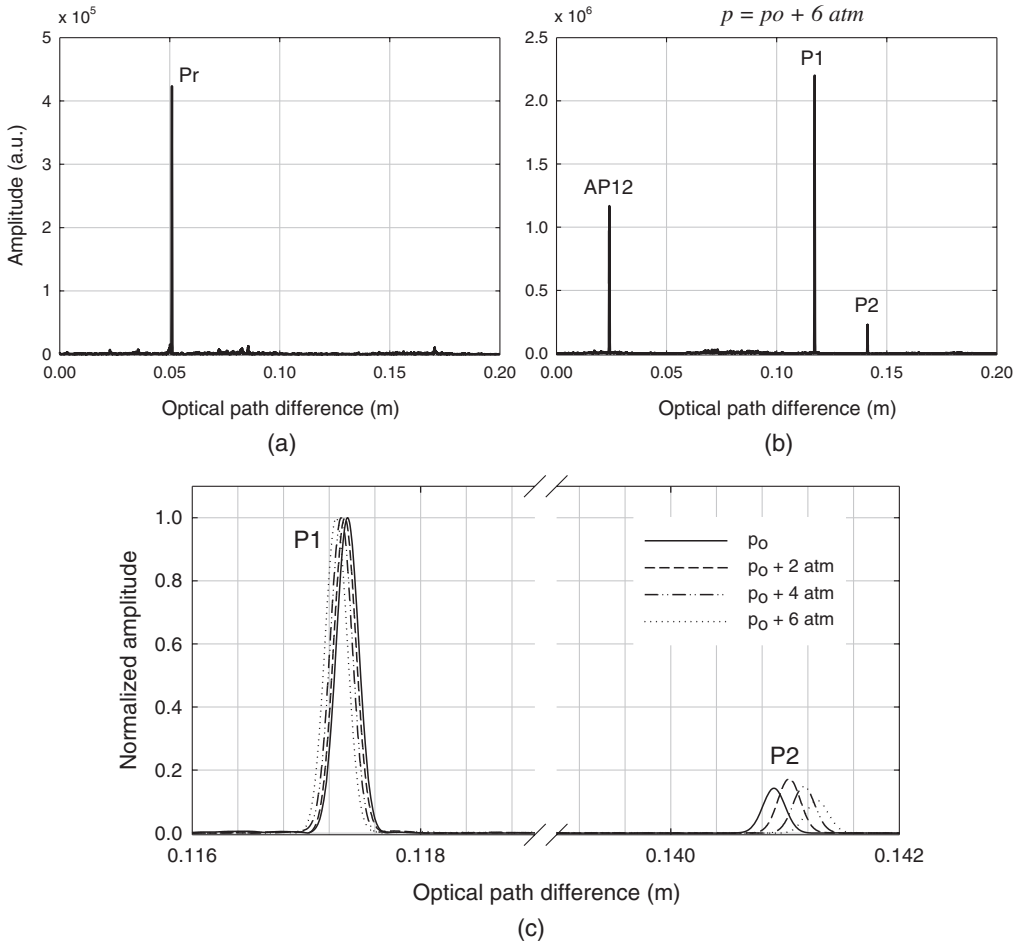

Fig. 9 Fourier transforms of the interference signals obtained when measuring microdeformations of a large opaque sample caused by applying pressure inside it.

above normal atmospheric pressure (p_0) was applied inside the constructed device. In Fig. 9(c), the enlargement of a sector of the Fourier transform is shown, where the changes experienced by peaks P_1 and P_2 can be observed as the pressure applied inside the cylinder increases. It can be clearly seen that P_1 (linked to deformation of face 1) moves less than P_2 (related to deformation of face 2), which is in perfect correspondence with the values obtained from the modeling performed.

It is important to highlight that, in addition to the total length of the object, it was possible to measure simultaneously and independently the deformations experienced by each of the opposite faces of the sample when they were subjected to certain mechanical stress. This confirms that the system is capable of being used in quality control applications, calibration, and characterization of some mechanical properties.

4 Conclusions

LCI is a nondestructive and noncontact measurement technique, highly adaptable to industrial conditions when using fiber-based measuring systems. In this work, we have demonstrated the feasibility of dimensionally characterizing large opaque samples using a scheme based on this technique, which employs a tunable light source combined with a Sagnac–Michelson configuration of the interferometric system. The proposed arrangement has a wide measuring range (several centimeters) with a constant high axial resolution. It was employed to measure different opaque objects up to about 7-cm thick. The method has certain limitations since not all types of samples can be analyzed. It can only be applied to those that have parallel faces since the

reflections of the light beams must return to the optical fiber, and therefore thickness measurements can only be made in the direction of the optical axis. Additionally, the implemented scheme was capable of simultaneously measuring microdeformations experienced by opposite faces of the samples, at the same time as the relatively large dimension or thickness. In this work, no lateral scans were performed because it was not intended to perform an analysis of the surface of the sample, but if necessary, the lateral resolution would be affected by the scanning system or translation system used. The simplicity of the proposed configuration privileges aspects such as robustness, reliability, and repeatability, which makes it appropriate to carry out dimensional characterization of large mechanical parts as those used in different industrial areas. The developed system can be used to perform profilometry of opaque samples, analysis of the dimensional behavior of mechanical pieces in production lines, or under mechanical efforts capable of introducing some deformations on them, etc.

Acknowledgments

This work was funded by Consejo Nacional de Investigaciones Científicas y Técnicas CONICET (PIP 112-201101-00397), Facultad de Ingeniería de la Universidad Nacional de la Plata (Proyecto I169), Comisión de Investigaciones Científicas de la Provincia de Buenos Aires CIC (Resoluciones Nos. 602/16 and 195/17), and Facultad Regional Delta, Universidad Tecnológica Nacional, Argentina (PID 2221). The authors wish to thank Mg. Andrea Pierre Castell from Centro de Investigación en Metrología y Calidad (CEMECA, CIC) for performing mechanical thickness measurements of opaque parts used in this work.

References

1. M. L. Dufour et al., "Low-coherence interferometry—an advanced technique for optical metrology in industry," *Insight* **47**(4), 216–219 (2005).
2. W. Drexler and J. G. Fujimoto, *Optical Coherence Tomography: Technology and Applications*, 2nd ed., Springer International Publishing, Switzerland (2015).
3. B. Grajciar et al., "High sensitive measurement of the human axial eye length in vivo with Fourier domain low coherence interferometry," *Opt. Express* **16**(4), 2405–2414 (2008).
4. G. J. Tearney et al., "System and method for identifying tissue using low-coherence interferometry," US Patent US 7,761,139 B2 (2010).
5. W. A. Reed, M. F. Yan, and M. J. Schnitzer, "Gradient-index fiber-optic microprobes for minimally invasive in vivo low-coherence interferometry," *Opt. Lett.* **27**(20), 1794–1796 (2002).
6. A. Hirai and H. Matsumoto, "Low-coherence tandem interferometer for measurement of group refractive index without knowledge of the thickness of the test sample," *Opt. Lett.* **28**(21), 2112–2114 (2003).
7. J. Kim, J. Han, and J. Jeong, "Accurate wavelength calibration method for spectrometer using low coherence interferometry," *J. Lightwave Technol.* **33**(16), 3413–3418 (2015).
8. R. Leitgeb, C. Hitzenberger, and A. Fercher, "Performance of Fourier domain vs time domain optical coherence tomography," *Opt. Express* **11**(8), 889–894 (2003).
9. A. B. Vakhtin et al., "Common-path interferometer for frequency-domain optical coherence tomography," *Appl. Opt.* **42**(34), 6953–6958 (2003).
10. S. Costantino, O. Martinez, and J. Torga, "Wide band interferometry for thickness measurement," *Opt. Express* **11**(8), 952–957 (2003).
11. S. Cerrotta, E. N. Morel, and J. R. Torga, "Scanning optical coherence tomography applied to the characterization of surfaces and coatings," *Procedia Mater. Sci.* **9**, 142–149 (2015).
12. E. N. Morel and J. R. Torga, "Simultaneous measurement of deformation and thickness change in polymer films," *Proc. SPIE* **6293**, 62930R (2006).
13. Z. Hu, Y. Pan, and A. M. Rollins, "Analytical model of spectrometer-based two-beam spectral interferometry," *Appl. Opt.* **46**(35), 8499–8505 (2007).
14. Z. Wang et al., "Cubic meter volume optical coherence tomography," *Optica* **3**(12), 1496–1503 (2016).

15. E. N. Morel and J. R. Torga, "Dimensional characterization of opaque samples with a ring interferometer," *Opt. Laser Eng.* **47**(5), 607–611 (2009).
16. E. N. Morel et al., "Application of a long-range swept source optical coherence tomography-based scheme for dimensional characterization of multilayer transparent objects," *Opt. Eng.* **56**(8), 084102 (2017).
17. E. N. Morel et al., "Interferometric system based on swept source optical coherence tomography scheme applied to the measurement of distances of industrial interest," *Opt. Eng.* **55**(1), 014105 (2016).
18. A. Giordana and R. Duchowicz, "Development and analysis of a simple tunable erbium ring laser," *Proc. SPIE* **8011**, 80115A (2011).
19. W. Young, R. Budynas, and A. Sadegh, *Roark's Fórmulas for Stress and Strain*, 8th ed., McGraw-Hill, New York (2011).
20. W. D. Pilkey, *Formulas for Stress, Strain, and Structural Matrices*, 2nd ed., John Wiley & Sons, Hoboken, New Jersey (2004).

Nélida A. Russo is a researcher at the Centro de Investigaciones Ópticas (CIOp) and member of the Commission of Scientific Research of Buenos Aires Province (CIC), Argentina. She is an electronic engineer graduated from the Faculty of Engineering of the La Plata National University (UNLP) in 1985. She received her PhD in engineering from the UNLP in 2006. She worked as an assistant professor of physics at the Faculty of Engineering of UNLP. Since 2018, she has led the Optical Fiber Group at CIOp. Her current research interests include optical fiber applications in sensors, lasers, and optical communications.

Eneas N. Morel is an electronic engineer, graduated from the Faculty of Engineering of the La Plata National University (UNLP) in 2003. He got his PhD from the Delta Regional Faculty of the National University of Technology in 2010. He is currently a researcher at the Laboratorio de Optoelectrónica y Metrología Aplicada, Facultad Regional Delta, National University of Technology and a member of CONICET (Consejo Nacional de Investigaciones Científicas y Técnicas), Argentina. His research focuses mainly on low-coherence interferometry (LCI) applied to general metrology, and optical coherence tomography (OCT) applied to the study of materials.

Jorge R. Torga obtained a degree in physics in 1992 and a PhD in sciences in 1997 from the University of Buenos Aires. He is currently a researcher at the Laboratorio de Optoelectrónica y Metrología Aplicada, Facultad Regional Delta, National University of Technology and a researcher at CONICET (Consejo Nacional de Investigaciones Científicas y Técnicas), Argentina. His research focuses mainly on OCT and LCI techniques.

Ricardo Duchowicz received his MS and PhD degrees in physics from UNLP, in 1977 and 1981, respectively. He was a professor at the National University of La Plata (Faculty of Engineering-UNLP) until 2018 and a researcher at the National Council for Scientific and Technical Research (CONICET) in Argentina from 1982 until now. In 1995, he cofounded the Fiber Optics Lab in the CIOp. He has published extensively on subjects related to laser and laser applications, in particular on fiber-optic lasers, fiber sensors, and pulse transmission in fiber-optic links.